the plant journal

SEB SOCIETY FOR EXPERIMENTAL BIOLOGY

The Plant Journal (2023) doi: 10.1111/tpj.16393

Immune activation during *Pseudomonas* infection causes local cell wall remodeling and alters AGP accumulation

Sang-Jin Kim[1,2,3,†], Deepak D. Bhandari[1,2,†], Rylee Sokoloski[1,2] and Federica Brandizzi[1,2,3,*]

[1]*Great Lakes Bioenergy Research Center, Michigan State University, East Lansing, MI 48824, USA,*
[2]*MSU-DOE Plant Research Laboratory, Michigan State University, East Lansing, MI 48824, USA, and*
[3]*Department of Plant Biology, Michigan State University, East Lansing, MI 48824, USA*

Received 15 December 2022; accepted 5 July 2023.
*For correspondence (e-mail fb@msu.edu)
†These authors contributed equally to this work.

SUMMARY

The plant cell boundary generally comprises constituents of the primary and secondary cell wall (CW) that are deposited sequentially during development. Although it is known that the CW acts as a barrier against phytopathogens and undergoes modifications to limit their invasion, the extent, sequence, and requirements of the pathogen-induced modifications of the CW components are still largely unknown, especially at the level of the polysaccharide fraction. To address this significant knowledge gap, we adopted the compatible *Pseudomonas syringae–Arabidopsis thaliana* system. We found that, despite systemic signaling actuation, *Pseudomonas* infection leads only to local CW modifications. Furthermore, by utilizing a combination of CW and immune signaling-deficient mutants infected with virulent or non-virulent bacteria, we demonstrated that the pathogen-induced changes in CW polysaccharides depend on the combination of pathogen virulence and the host's ability to mount an immune response. This results in a pathogen-driven accumulation of CW hexoses, such as galactose, and an immune signaling-dependent increase in CW pentoses, mainly arabinose, and xylose. Our analyses of CW changes during disease progression also revealed a distinct spatiotemporal pattern of arabinogalactan protein (AGP) deposition and significant modifications of rhamnogalacturonan sidechains. Furthermore, genetic analyses demonstrated a critical role of AGPs, specifically of the Arabinoxylan Pectin Arabinogalactan Protein1, in limiting pathogen growth. Collectively, our results provide evidence for the actuation of significant remodeling of CW polysaccharides in a compatible host-pathogen interaction, and, by identifying AGPs as critical elements of the CW in plant defense, they pinpoint opportunities to improve plants against diverse pathogens.

Keywords: plant immunity, cell wall, plant-microbe interactions, arabinogalactan proteins, *Pseudomonas syringae*.

INTRODUCTION

During development, plant cells generally deposit a polysaccharide-rich primary cell wall (CW) prior to the deposition of a lignin-rich secondary CW, which occurs once cell elongation is concluded. The major non-lignin components of the dicot CW comprise three major components: cellulose, hemicellulose (xyloglucan), and pectins, such as homogalacturonan (HG), rhamnogalacturonan-I and II (RG-I and II). The CW also contains proteoglycans, such as extensins and arabinogalactan proteins (AGPs) (Borassi et al., 2016; Cannon et al., 2008; Showalter & Basu, 2016; Tan et al., 2013). While the role of these proteoglycans is not well understood, emerging evidence suggests that they play important roles in biotic and abiotic stresses (Mareri et al., 2019).

The CW is actively modified during plant development and in response to biotic and abiotic stresses, and signals arising from CW changes act as cues for transcriptional reprogramming events that influence plant growth and stress responses (De Lorenzo et al., 2019; Pontiggia et al., 2020; Wolf, 2022). Therefore, perturbations in either the composition or structure of the CW can affect plant fitness and/or pathogen resistance (Bethke et al., 2015; Engelsdorf et al., 2017; Gille & Pauly, 2012; Hernández-Blanco et al., 2007; Lionetti et al., 2012; Molina et al., 2021; Pogorelko et al., 2013; Swaminathan et al., 2022; Vogel et al., 2004). A recent study on Arabidopsis roots suggests that plant cells activate immunity upon receiving dual signals of damage and pathogen presence (Zhou et al., 2020). Thus, changes in CW, either pre- or post-infection, have a bearing on

pathogen resistance (De Lorenzo et al., 2019; Dora et al., 2022; Molina et al., 2021; Wan et al., 2021).

The plant immune system broadly functions at two interfaces: (i) at the plasma membrane (PM), where conserved microbial signatures (e.g., flagellin and chitin) or damage-associated molecules (e.g., CW-derived oligogalacturonides, extracellular bioactive molecules) are recognized by cell-surface pattern recognition receptors; and (ii) inside the cell, where pathogen-secreted effectors are recognized by plant resistance proteins. Immunity activated by cell-surface pattern recognition receptors is termed "pattern-triggered immunity" (PTI), while immunity activated upon recognition of intracellular effectors is known as "effector-triggered immunity" (ETI) (Couto & Zipfel, 2016; Jones & Dangl, 2006; Thordal-Christensen, 2020; van der Burgh & Joosten, 2019). Basal immunity is a defense response induced upon infection by a virulent pathogen, which limits pathogen growth (Lapin et al., 2020). Initiation of immunity leads to reprogramming of the plant transcriptome and activation of multiple signaling cascades. As a result, endomembrane traffic and hormonal pathways are altered, and, in addition to localized cell death, CW lignification can take place (Bhandari & Brandizzi, 2020; Cui et al., 2015; Lee et al., 2019; Tsuda et al., 2009). Although a reinforcement of the CW through the accumulation of lignin and other phenolics most likely restricts pathogen movement and/or proliferation (Lee et al., 2019; Underwood, 2012), it is still to be systematically established whether other CW components are qualitatively and quantitatively altered upon infection. Likewise, whether specific changes in CW upon infection drive successful plant immunity is yet to be defined.

Resistance to biotrophic pathogens as well as hemibiotrophic bacteria, such as *Pseudomonas syringae* (*Pst*), is largely mediated by the phytohormone salicylic acid (SA), although SA-independent signaling pathways have also been identified (Ding & Ding, 2020; Tsuda et al., 2009; Zhang & Li, 2019). SA is also essential for initiating systemic acquired resistance (SAR). SAR is an immune response generated in the local tissue upon pathogen infection and transmits defense signals to systemic tissues, resulting in broad resistance at the organismal level (Hartmann & Zeier, 2019). Signaling molecules that initiate and perceive systemic signals have been recently discovered (Hartmann et al., 2018; Hartmann & Zeier, 2019); however, whether SAR activation modifies CW in systemic tissues is still unknown.

In this study, we used the well-established *Pst-Arabidopsis thaliana* pathosystem to investigate changes in CW polysaccharides during a compatible interaction. We adopted *Pst DC3000* because this pathogen does not cause lignin accumulation (Lee et al., 2019), and therefore, would allow us to monitor changes in CW polysaccharides during infection. We observed that upon infection by a compatible pathogen, the host CW undergoes extensive remodeling. Most notably, we also found that a virulent pathogen challenge in leaves leads to an increased deposition of pentoses (i.e., arabinose and xylose) into the CW of epidermal cells and mesophyll cells, a phenomenon that requires the activation of host basal immune signaling. We also demonstrated that the changes in pentose levels are controlled by immune signaling in spatially defined regions of the invaded tissue rather than systemically. By monitoring these CW changes, we discovered a *Pst*-driven accumulation of galactans, which is attenuated by immune activation, and identified a critical role for Arabinoxylan Pectin Arabinogalactan Protein1 (APAP1) in successfully antagonizing pathogen infection during CW remodeling. Our results provide new insights into the complex CW modifications occurring in a compatible plant-pathogen interaction at a detailed spatiotemporal resolution and advance current knowledge on the components necessary for an effective plant defense against phytopathogens.

RESULTS

Pst infection leads to CW changes in local but not systemic tissues

To monitor changes in CW composition in local and systemic tissues during a compatible interaction, we infected four-week-old Arabidopsis Col-0 (from here on Col) leaves with the biotrophic pathogen *Pst DC3000* (from here on *Pst*). Samples were harvested 3 days post-infection (dpi) from both the infiltrated leaf (local) and uninfiltrated adjacent leaves (systemic). The neutral sugar composition (NSC) of the CW of both local and systemic tissues was analyzed in de-starched alcohol insoluble residue (AIR). In the local tissue, we found that pathogen challenge led to a significant increase in all the measured sugars, indicative of marked pathogen-induced changes in the CW NSC (Figure 1A). Next, to assay the NSC of the systemic tissue, we analyzed an uninfiltrated adjacent leaf of each infected plant. Upon bacterial infection, systemic signaling molecules accumulate in systemic tissues by 1 dpi up to 3 dpi (Hartmann et al., 2018). When we analyzed the NSC of systemic tissue at 3 dpi, we found no significant changes compared to mock samples (Figure 1B). These results indicate that, in a compatible interaction, by the time systemic signaling has already peaked in systemic tissues, the CW NSC is significantly altered only in the infected tissues.

Changes in CW composition correlate with pathogen virulence and host immune signaling

The identification of CW NSC alteration caused locally by *Pst* infection led us to test if such changes could be determined by either host immune signaling and/or pathogen virulence. To do so, we adopted the established

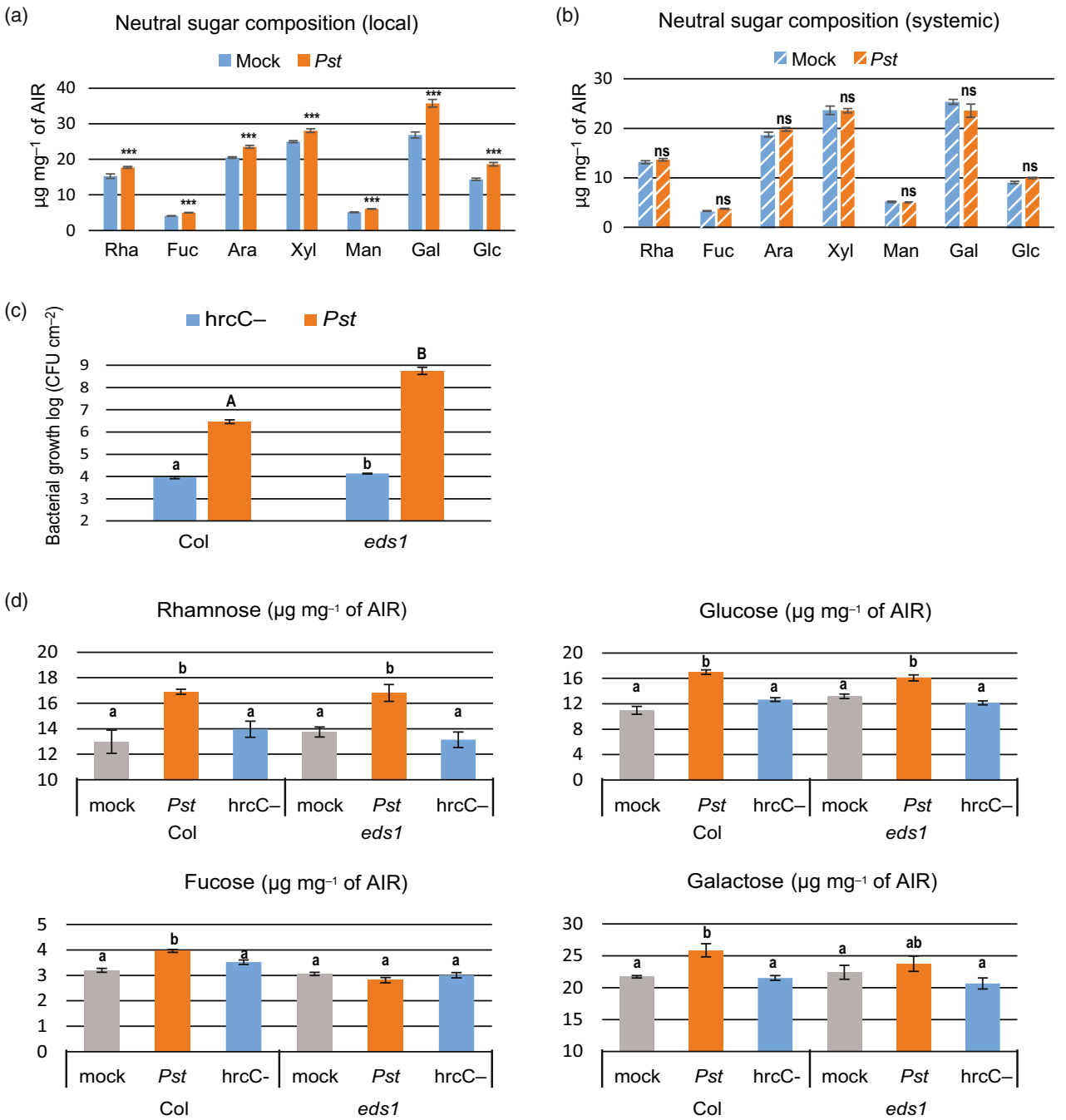

Figure 1. *Pseudomonas syringae* infection leads to CW changes in local but not systemic tissue.
(a, b) Four-week-old Col Arabidopsis plants were infiltrated with either mock (10 mM $MgCl_2$) or *Pst*. Infiltrated leaves [local (A)] and adjacent uninfiltrated leaves [systemic (b)] were harvested 3 dpi, and the NSC was analyzed. Bars represent mean of three independent replicates ± SD. Differences between treatments were determined by student's *t*-test ($P < 0.05$).
(c) Four-week-old Arabidopsis plants of the indicated genotypes were infiltrated with either *Pst* hrcC− or *Pst* and bacterial titers determined at 3 dpi. Bars represent mean of three biological replicates ± SE. Differences between genotypes, within treatment, were determined by student's *t*-test ($P < 0.05$).
(d) Four-week-old Arabidopsis plants were infiltrated with either mock (10 mM $MgCl_2$), *Pst* hrcC−, or *Pst*. Infiltrated leaves were harvested 3 days later and the NSC was analyzed. Bars represent mean of three replicates ± SD. Differences between treatments were determined by two-way ANOVA ($P < 0.05$).

immune-compromised Arabidopsis mutants that are hypersusceptible to *Pst*: *eds1-2* (*eds1* from here on), a mutant lacking a central immune signaling component (Aarts et al., 1998; Lapin et al., 2020), and *sid2-2* (from here on *sid2*), a mutant deficient in SA biosynthesis (Dewdney et al., 2000). As pathogens, we used *Pst*, *Pst* hrcC− (a *Pst*

mutant with reduced virulence due to a defective type-III secretion system (T3SS) but activates PTI) and *Pst* DC3000 Δcor- (a *Pst* mutant lacking coronatine, a jasmonic acid (JA)-mimic virulence factor) (Hauck et al., 2003; Yuan & He, 1996). Coronatine is a phytotoxin used by *Pst* to subvert host immune responses by antagonizing JA pathways (Cui et al., 2018). Both *Pst* hrcC− and *Pst* DC3000 Δcor- are less virulent than *Pst* and their growth in Col is reduced compared to *Pst* (Figure 1C; Figure S1).

When we analyzed the CW NSC after infiltration of Col and *eds1* with either mock, *Pst*, or *Pst* hrcC−, we found that, except for fucose, *Pst* infection led to a significant increase in hexoses (glucose, galactose, and mannose), deoxy-hexoses (rhamnose) in both Col and *eds1* (Figure 1D, Figure S1), indicating that the observed pathogen-driven increased accumulation of hexoses occurs independently of host immune signaling. Interestingly, the levels of cellulose, the most abundant CW polysaccharide, were not changed upon *Pst* infection in Col, while a slight decrease was observed in *eds1* (Figure S1b). The decrease of cellulose levels in *eds1* was observed upon infection with *Pst* hrcC−, suggesting that this is a response shared in PTI and basal resistance. We further tested if the levels of uronic acids, which are indicative of the abundance of pectic polysaccharides, were also increased upon *Pst* infection and found that, upon *Pst* infection, they were increased in both Col and *eds1* compared to mock-treated plants (Figure S1f). Thus, a large part of CW changes upon infection are pathogen driven. To further decipher the drivers of CW modifications during *Pst* infection, we assayed the NSC of Col and *eds1* plants infected with *Pst* DC3000 Δcor- (Figure S1). Infection with *Pst* DC3000 Δcor- resulted in increased rhamnose, glucose, and fucose levels but not mannose and galactose signifying a partial dependence of the accumulation of CW components upon the pathogen-elicited coronatine during infection. Furthermore, we established that contrary to the marked changes in the CW hexoses upon challenge with the virulent *Pst* or *Pst* DC3000 Δcor-, no substantial changes occurred upon infection with *Pst* hrcC− compared to mock-treated samples (Figure 1C,D; Figure S1). Significantly, upon *Pst* and *Pst* DC3000 Δcor- infection, a clear increase in pentose levels (i.e., arabinose and xylose) was observed in Col, but not in the hypersusceptible *eds1* (Figure 2A; Figure S1). Also, an increase in pentose levels was not observed upon *Pst* hrcC− infection in both Col and *eds1* compared to mock-treated plants (Figure 2A). Taken together, these results indicate that, upon a compatible pathogen challenge, increased deposition of CW neutral sugars is linked to pathogen virulence, specifically to *Pst*-secreted effectors; however, plant immune signaling is required for an increase in the deposition of pentoses.

The results obtained with *Pst* DC3000 Δcor- infection indicate that coronatine plays a role in *Pst*-driven CW modifications. However, to avoid complications due to the SA-JA antagonism, we focused on CW modifications during *Pst* infection to obtain a comprehensive understanding of pathogen-driven CW changes.

Because our results showed that increased CW pentose deposition relies on the host immune response (Figure 2A), we next aimed to test whether reduced levels of arabinose or xylose in the CW would impair resistance to virulent bacteria. To do so, we analyzed Arabidopsis mutants that are defective in UDP-arabinose or xyloglucan production. Arabinose is commonly found in the arabinan side chain of RG-I or AGPs (Showalter & Basu, 2016). Xylose is a major component of xyloglucan in the primary CW and constitutes the bulk of the xylan backbone and xylogalacturonan in Arabidopsis (Scheller & Ulvskov, 2010). For our analyses, we used a knockout (KO) mutant of *MURUS4* (*mur4*) (Burget et al., 2003), an epimerase catalyzing the interconversion of UDP-xylose to UDP-arabinose. This mutant has ~50% reduced arabinose in the leaf NSC compared to Col (Burget et al., 2003). We also used a quintuple mutant of *Cellulose synthase like-C 4,5,6,8,12* genes (*cslc*), which has no detectable xyloglucan (Kim et al., 2020). Upon infiltration with *Pst*, we found that both *mur4* and *cslc* displayed increased resistance compared to Col, while *eds1* and *sid2* showed increased susceptibility as expected (Figure 2B). We next analyzed the CW NSC of pathogen-infiltrated leaves of Col, *mur4*, *cslc*, *sid2*, and *eds1* plants. Although *mur4* and *cslc* had lower basal levels of arabinose and xylose compared to Col, respectively, upon *Pst* infection, both mutants showed a significant increase in pentose levels, as follows: we observed a greater increase of xylose in *mur4* than in Col; conversely, *cslc* showed a greater increase in arabinose compared to all the other genotypes (Figure 2C). Pentose levels were not largely changed in *eds1*, which showed a slight reduction in arabinose, and in the susceptible *sid2* (Figure 2C). Together, these results show that reduced basal levels of either xylose (no xyloglucan in *cslc*) or arabinose (reduced levels of arabinan in *mur4*) do not impair host defense. These data also underscore the importance of pentose deposition in the CW for defense upon immune activation, as evidenced by an enhanced resistance of *mur4* and *cslc*, which showed increased xylose and arabinose levels, respectively.

Immunity activation results in reduced arabinan levels and increased AGP and galactan deposition in the CW

To deepen knowledge about the modifications of the observed CW NSC changes upon pathogen challenge (Figures 1 and 2), especially about how pentoses may be incorporated into the existing CW microstructures, we investigated the distribution of xylose and arabinose in the two CW matrix fractions by sequential extraction of the soluble fractions from AIR of *Pst*-challenged leaves. We

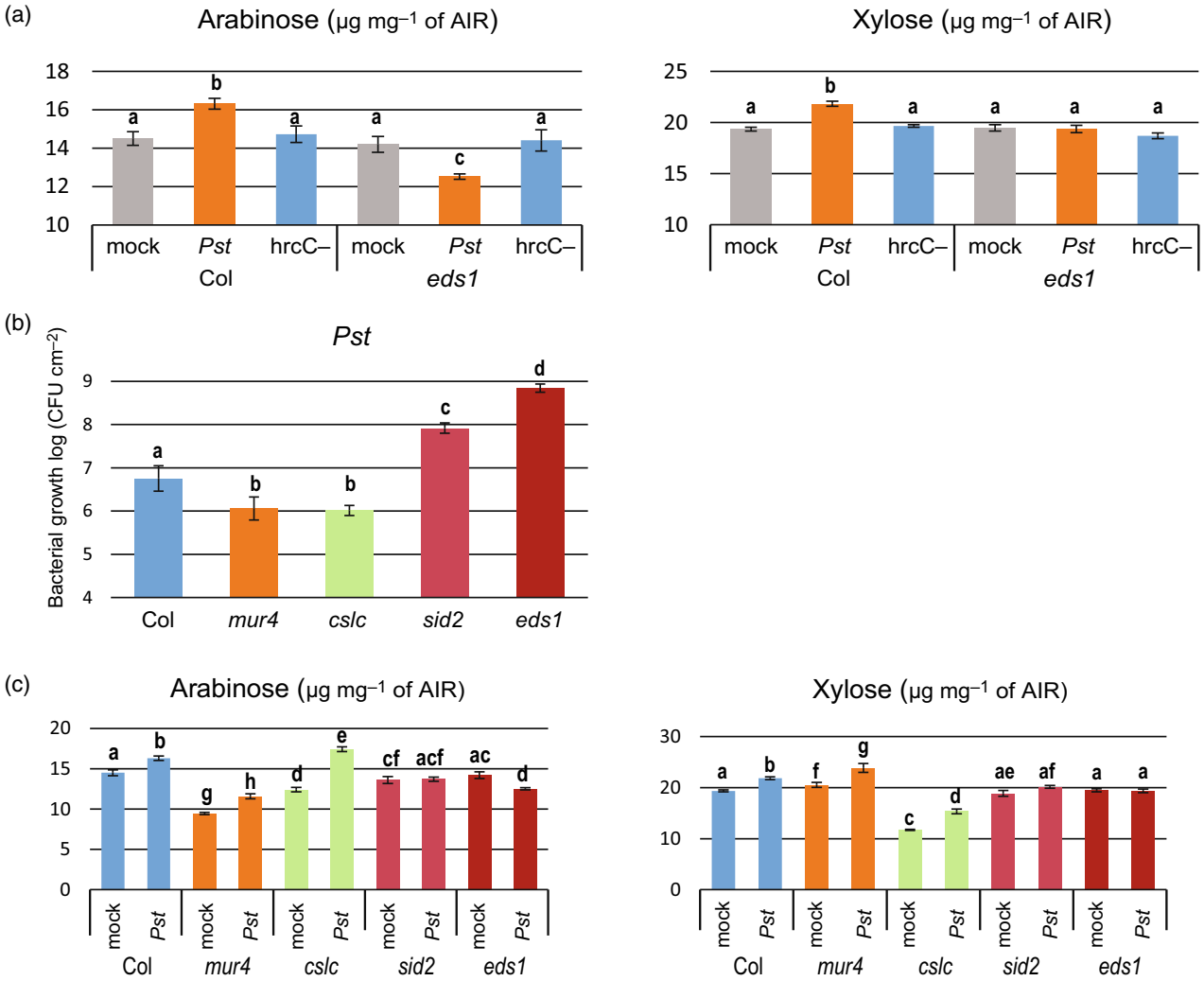

Figure 2. Changes in CW composition correlate with pathogen virulence and host resistance.
(a) Four-week-old Arabidopsis plants were infiltrated with either mock (10 mM $MgCl_2$), *Pst* or *Pst* hrcC−. Infiltrated leaves were harvested 3 dpi and NSC was analyzed. Bars represent the mean of three independent replicates ± SD. Differences between treatments were determined by two-way ANOVA ($P < 0.05$).
(b) Four-week-old Arabidopsis plants of the indicated genotypes were infiltrated with *Pst* and bacterial titers determined at 3 dpi. Bars represent the mean of three biological replicates ± SE. Differences between genotypes within treatment were determined using one-way ANOVA (Tukey's HSD, $P < 0.05$).
(c) Four-week-old Arabidopsis plants were infiltrated with either mock (10 mM $MgCl_2$) or *Pst*. Infiltrated leaves were harvested 3 days later and NSC was analyzed. Bars represent the mean of three replicates ± SD. Differences between treatments were determined by two-way ANOVA ($P < 0.05$).

focused on the 1 M KOH fraction to extract pectin and hemicellulose weakly associated with other CW components, and the 4 M KOH fraction to extract pectin and hemicellulose tightly associated with other CW components. We then used quantitative dot blotting analyses with antibodies recognizing specific epitopes of CW polysaccharides. First, we used the LM15 antibody specific to xylosyl residues in the XXXG motif of xyloglucan and the LM10 antibody specific to unsubstituted xylan to gather insights into the xylose distribution in the CW. In our CW composition analyses, we found increased xylose levels in *Pst*-infected Col (Figure 1A), but we did not observe a corresponding increase of either xyloglucan (LM15) or unsubstituted xylan (LM10) (Marcus et al., 2008; McCartney et al., 2005) (Figure S2). Next, we used the LM2 antibody which is specific to the ß-linked glucuronic acid of AGP, the LM6 antibody which is specific to the RG-I arabinan side chain, and the LM5 antibody which is specific to the RG-I galactan side chain, to detect the the levels of AGP, RG-I arabinan, and RG-I galactan, respectively (Jones et al., 1997; Smallwood et al., 1996; Willats et al., 1998; Yates et al., 1996). In both AIR fractions, we observed a marked increase of LM2 (AGP) signal in Col infected with *Pst* compared to mock, while in *Pst* hrcC− challenged leaves, the LM2 signal was comparable to mock (Figure 3). Remarkably, *Pst* infection led to an increase in AGP levels even in the 4 M KOH extract (Figure 3b). Conversely, minimal levels of AGPs were detected in 4 M KOH mock samples. Upon infection,

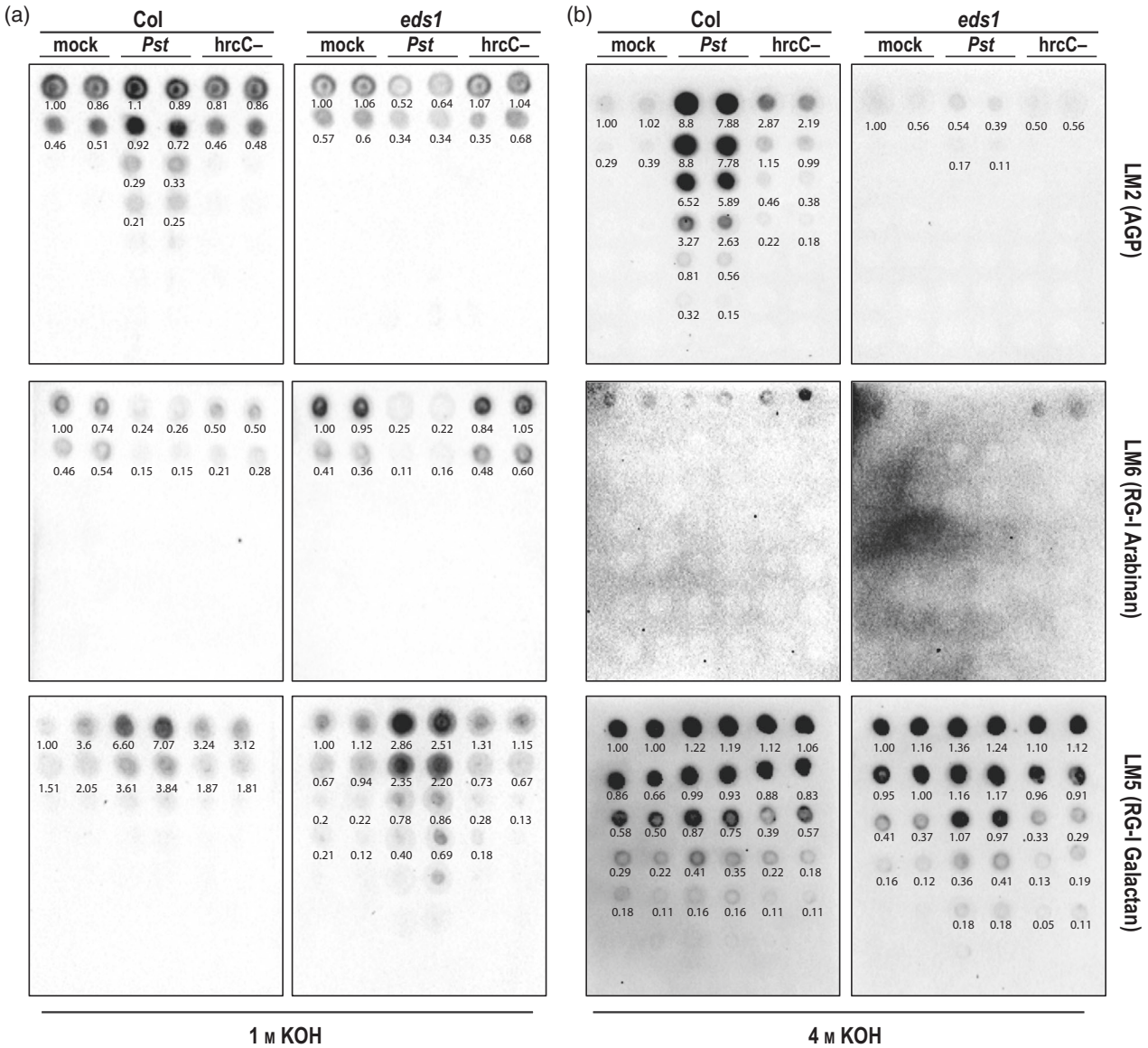

Figure 3. Differential sequestration of arabinose upon *Pseudomonas* infection.
Four-week-old Arabidopsis leaves of the indicated genotypes were infiltrated with either mock (10 mM $MgCl_2$), *Pst* hrcC−, or *Pst*. Infiltrated leaves were harvested 3 days later and AIR was extracted. Sequential extractions using (a) 1 M KOH and (b) 4 M KOH were performed on AIR, followed by dot-blot analyses on 2 μg de-starched AIR with LM2 (AGP), LM6 (alpha-1,5-arabinan), LM5 (beta-1,4-galactan). Values represent the relative quantification of each dot-blot sample normalized to undiluted mock samples (value set to 1) within each blot.

no changes in the LM2 signal were observed in the *Pst* hypersusceptible *eds1* and *sid2* mutants (Figure 3; Figure S3). Furthermore, the AGP levels in the extracts of the *Pst*-resistant mutants, *mur4*, and *cslc*, were similar to Col, showing an increase of LM2 signal upon *Pst* infection (Figure S3). These results indicate that, upon *Pst* infection, quantitative and qualitative changes occur in the CW NSC with an increased accumulation of arabinose into AGP, and that such accumulation depends on the pathogen and plant immune responses.

Next, using LM6 antibody (RG-I arabinan), we found that the RG-I arabinan levels were decreased, in stark contrast to AGP deposition (Figure 3). A reduction of LM6 signal was also observed in *eds1* and *cslc* but not in *sid2* (Figure 3; Figure S3). Although we did not verify any differences in the levels of arabinose in the NSC analysis upon infection with *Pst* hrcC− in Col, we found a slight reduction in the arabinan levels in Col. The levels of arabinan in *eds1* were not changed upon infection with *Pst* hrcC−, consistent with the results of the NSC analysis (Figures 2A and 3), suggesting that pathogen-elicited effectors are involved in the depletion of RG-I arabinan from the CW. These results indicate that *Pst* infection influences arabinose metabolism possibly by altering both the synthesis and

degradation of molecules containing arabinose (i.e., AGP and RG-I) in an immune-dependent manner. Importantly, these results also suggest that, upon *Pst* infection, the increased pool of arabinose-containing carbohydrates is not equally utilized to produce AGP and arabinan. Specifically, a preferential sequestration of arabinose towards an increased AGP deposition and a concomitant removal of arabinan from RG-I appear to take place. In addition to the changes in the levels of AGP and RG-I arabinan, we observed increased levels of RG-I galactan (LM5) in both Col-0 and *eds1*, indicating a pathogen-driven but host-signaling independent activation of RG-I galactan deposition.

The loss of the AGP APAP1 leads to increased susceptibility to *Pst*

Because we observed significant changes in AGP deposition in the CW upon *Pst* infection in Col (Figure 3), we hypothesized that plants with defective AGP deposition would be vulnerable to pathogens. Therefore, to test our hypothesis, we infected *Pst* into KO mutants of *AGP17*, *AGP18*, and *APAP1* (i.e., *agp17*, *agp18*, and *apap1-4*) (Gaspar et al., 2004; Tan et al., 2013; Yang & Showalter, 2007). AGP17 and AGP18 are anchored to the PM by a glycosyl-phosphatidylinositol anchor (Zhang et al., 2011). APAP1 contains the AGP57Ca core protein that cross-links pectin and hemicellulose, resulting in a large proteoglycan (Tan et al., 2013). In addition, we included the arabinose biosynthesis KO mutant *arabinokinase1* (*ara1*), which has reduced levels of arabinose in the CW (Sherson et al., 1999), as well as *mur4* and *sid2* as controls. Upon *Pst* infection, we did not observe any differences in bacterial growth between *agp17*, *agp18*, and Col, while the *apap1* and *sid2* mutants supported 5- to 7-fold and 10- to 12-fold increase in bacterial colonies compared to Col, respectively (Figure 4). Conversely, *ara1* and *mur4* showed increased resistance to *Pst* (Figure 4), suggesting that *ara1* may have an AGP increase upon pathogen infection similar to *mur4*. These results indicate that an accumulation of a specific form of AGP upon pathogen infection may be responsible for the increased resistance. Furthermore, the significant decrease of resistance in *apap1-4* underscores the unique role of APAP1 among the AGPs in resistance to *Pst*.

SA has a limited role in immunity-induced CW modifications

Upon *Pst* infection, SA plays an important role in upregulating defense pathways for limiting pathogen growth (Tsuda et al., 2009; Wildermuth et al., 2002). We observed that *Pst* infection led to marked modifications in the CW NSC of Col but not *sid2* (Figure 3; Figure S3). Therefore, we next aimed to test if SA-mediated defense responses were causative of the CW modifications upon pathogen infection. To do so, we grew Col and *non-expresser of PR1*

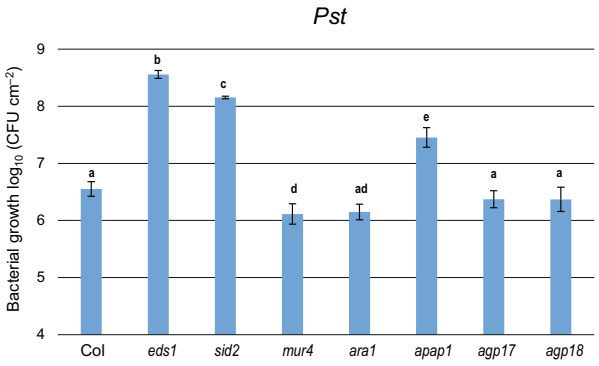

Figure 4. The loss of the AGP APAP1 leads to increased susceptibility to *P. syringae*.
Four-week-old Arabidopsis plants of the indicated genotypes were infiltrated with *Pst* and bacterial titers were determined at 3 dpi. Bars represent the mean of three biological replicates ± SE. Differences between genotypes were determined by one-way ANOVA (Tukey's HSD, $P < 0.05$).

(*npr1*), a SA receptor mutant (Manohar et al., 2015; Wu et al., 2012), on plates supplemented with SA. The efficacy of SA treatment was verified by measuring the expression of the SA marker gene *PR1* (Sels et al., 2008), which was increased in Col but not in *npr1* (Figure 5a). We then sequentially extracted: pectin/chelating agent-soluble solids (ChASS), 1 and 4 M KOH fractions for analyses with epitope-specific antibodies. Because of the verified increase in AGP levels in the CW upon immune activation (Figure 3), and the key role of SA in bacterial immunity, we hypothesized that SA signaling would also play a role in AGP deposition. However, in both Col and *npr1* backgrounds we did not observe any SA-induced change in AGP (LM2) and galactan RG-I (LM5) in all the fractions tested (Figure 5b). Rather we found that SA treatment led to a decrease of RG-I arabinan (LM6) in the pectin fraction, but not in the other fractions (Figure 5b), suggesting a limited role of SA in CW remodeling. Taken together, the results from *Pst* infection (Figure 3) and SA treatment (Figure 5) indicate the involvement of distinct immune-signaling pathways to modify specific CW polymers.

Spatio-temporal changes in the CW correlate with host resistance and bacterial proliferation

Next, we aimed to test if CW remodeling occurred concurrently with bacterial proliferation and the associated immune response, and we monitored the dynamics of CW remodeling focusing on AGP and pectin over the course of pathogen infection. To do so, we infiltrated Col and *eds1* leaves with *Pst*, harvested samples at 1, 2, and 3 dpi, and monitored the increase in bacterial growth and expression of the defense marker *PR1* (Figure 6a; Figure S7a). To better understand *Pst*-driven modifications in different CW fractions, we sequentially extracted pectin-enriched ChASS fractions prior to 1 and 4 M KOH fractions. At 2 and 3 dpi, we observed a clear increase in AGP levels concomitant

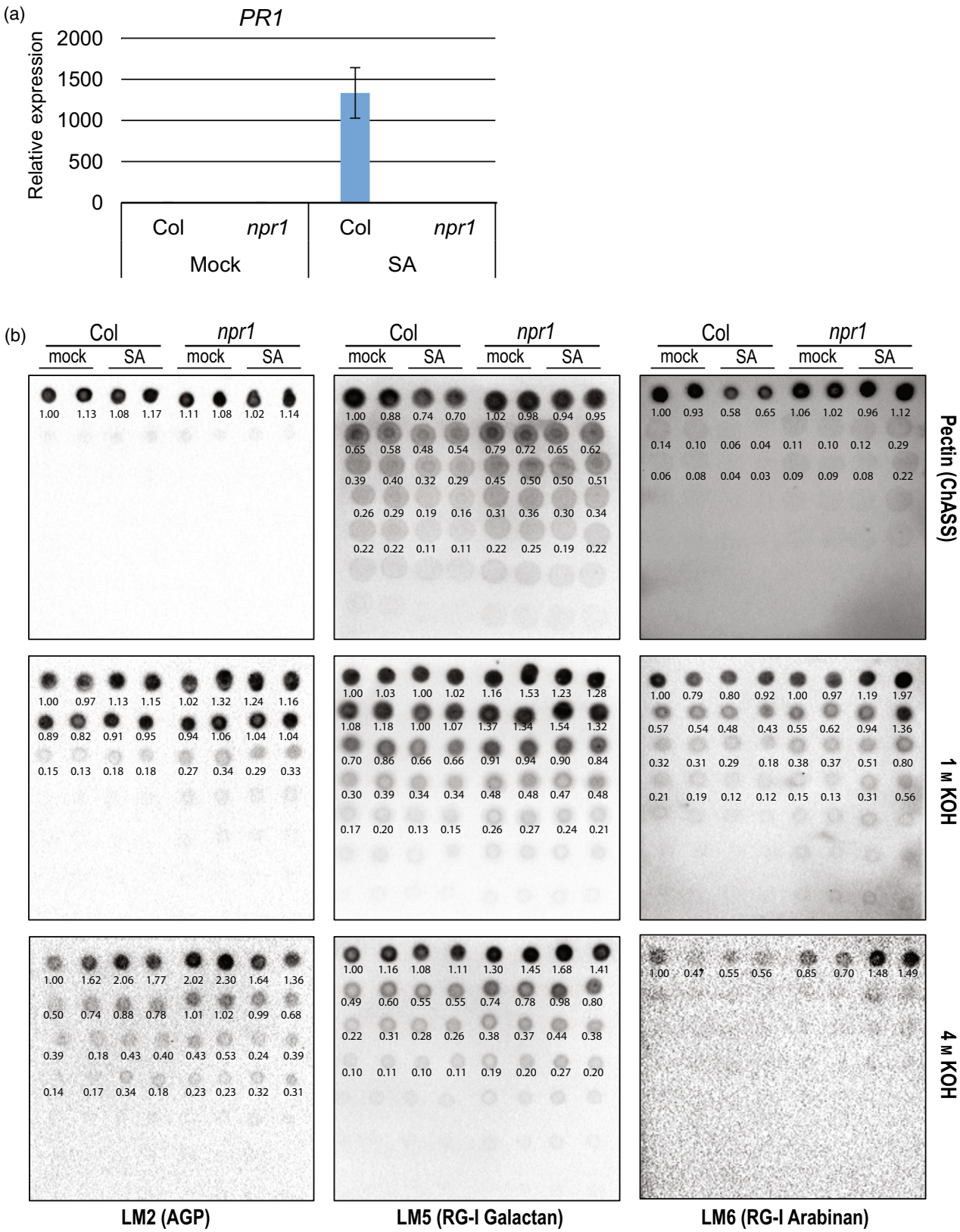

Figure 5. SA leads to selective depletion of arabinan in rhamnogalacturonan-I.
Ten-day-old Arabidopsis seedlings of the indicated genotypes were grown for 3 days on plates supplemented with 50 μM SA. (a) *PR1* transcripts were measured using qRT-PCR. Bars represent means ± SE of three biological replicates. (b) AIR was extracted from leaf tissue. Sequential extractions of pectin (ChASS), 1 M KOH, and 4 M KOH fractions were performed, followed by dot-blot analyses on 2 μg de-starched AIR with LM2 (AGP), LM6 (alpha-1,5-arabinan), LM5 (beta-1,4-galactan). Values represent the relative quantification of each dot-blot sample normalized to undiluted mock samples (value set to 1) within each blot.

with bacterial growth in all three Col CW fractions (i.e., pectin/ChASS, 1, and 4 M KOH) (Figure 6b; Figures S4 and S5) while a slight decrease was observed in AGP levels in the 1 M KOH fraction of the hypersusceptible *eds1* mutant. The observed temporal deposition of AGPs led us to examine if the dynamics of AGP deposition correlated with an induction of AGP biosynthesis genes. We selected candidates induced during biotic stress from the *Galactosyl transferase* (*GALT*) and *Prolyl-4-hydroxylase* (*P4H*) families based on previous reports and a public gene expression database (BAR) (Kaur et al., 2021; Vlad et al., 2007; Winter et al., 2007). Significant differences in the expression of the tested genes were observed between Col and *eds1* at 2 dpi compared to mock-treated samples. We observed an increase in the expression of *GALT7*, *GALT8*, and *GALT9* at 2 dpi compared to mock in Col but not in *eds1* (Figure S7b). However, *P4H*s were induced at 2 dpi both in Col and *eds1*, indicating *GALT*s could relate to AGP deposition during immune activation. Together these results (Figures 3 and 6; Figures S4 and S5) underscore a need for immune signaling leading to gene reprogramming and increased AGP deposition in specific CW fractions.

We next focused on changes in galactan levels, which increased in both Col and *eds1* upon *Pst* infection (Figure 3). In both the ChASS and 4 M fractions of Col and *eds1*, we observed a discernible decrease in galactan levels at 1 dpi compared to mock-treated leaves, followed by a notable increase at 2 and 3 dpi (Figures S4 and S5). In contrast, in Col 1 M fraction, we observed an increase in galactan levels early in the infection (1 dpi) followed by a peak at 2 dpi and a decrease by 3 dpi (Figure 6), suggesting the occurrence of a pathogen-driven increase in galactan levels early in infection that is attenuated later (Figure 6). Consistent with this possibility, in *eds1* we found a steady increase in galactan deposition during the infection (Figure 6). Similar to the AGP deposition, the increase in galactan deposition was associated with an increase in the expression of *Galactan synthase* genes (*GALS1, 2, 3*) upon *Pst* infection in both Col and *eds1* (Figure S7c).

In contrast to the decrease in arabinan levels when 1 M KOH fraction was not depleted of ChASS fraction (Figure 3), we observed an increase in arabinan levels in the 1 M KOH fraction stripped of the ChASS fraction (Figure 6). As expected, decreased arabinan levels were observed in Col ChASS fraction, indicating a higher level of RG-I arabinan depletion in the pectic fraction, and suggesting that the composition of CW polysaccharides can change dynamically during infection. Different from the activated AGP and galactan biosynthesis pathways upon *Pst* infection, we found that *Pst*-induced changes in the expression of genes regulating arabinan did not correlate with observed changes in arabinan levels (Figure S7c). The observed modifications in RG-I suggest that galactan and arabinan may be independently modified in RG-I or masked by other factors in the CW during *Pst* infection.

The major pectic polysaccharide in Arabidopsis primary CW is HG. Because RG-I was modified significantly upon *Pst* infection (Figure 6), we evaluated changes in HG upon *Pst* infection using ChASS fraction. We monitored HG using JIM5 and JIM7 antibodies, which recognize lowly methylesterified HG and highly methylesterified HG, respectively. We observed an increase of lowly methylesterified HG (JIM5) and a decrease of highly methylesterified HG (JIM7) labeling 2 dpi onwards (Figure S6). Although the verified changes in JIM5 and JIM7 labeling upon *Pst* infection indicate that either HG is demethylated with no overall changes in the levels of HG or that the biosynthesis and degradation of HG are balanced in the pectin-enriched fraction, they support that *Pst* infection leads to pectin demethylesterification.

CW modifications occur at the sites where pathogen contacts the CW

During infection, *Pst* initially comes in contact with the epidermal layer and spongy mesophyll cells (Xin et al., 2018). Therefore, we next aimed to understand if the observed CW changes (Figures 1–6) would predominantly affect these two cell layers in the leaf. To do so, we generated transverse sections of mock and *Pst*-infected leaves of Col and *eds1* for immunofluorescence analyses with antibodies for AGP (LM2), galactan (LM5), and xyloglucan (LM15). We did not observe differences in antibody labeling pattern between Col and *eds1* mock-treated samples, which showed uniform labeling of LM2, LM5, and LM15 (Figure 7a). In line with the dot-blotting results and CW composition data (Figures 2, 3 and 6), we found that in Col *Pst* infection led to changes in the labeling pattern of LM2, LM5, and LM15 specifically at the spongy mesophyll and epidermal cells (Figure 7a; Figure S8). In contrast, we did not observe such a distinct labeling pattern in *eds1* (Figure 7a). Interestingly, in both pathogen-unchallenged Col and *eds1* tissues, we detected labelling of AGP in punctate structures; however, we found that *Pst* infection resulted in a uniform labeling of AGP across abaxial cells

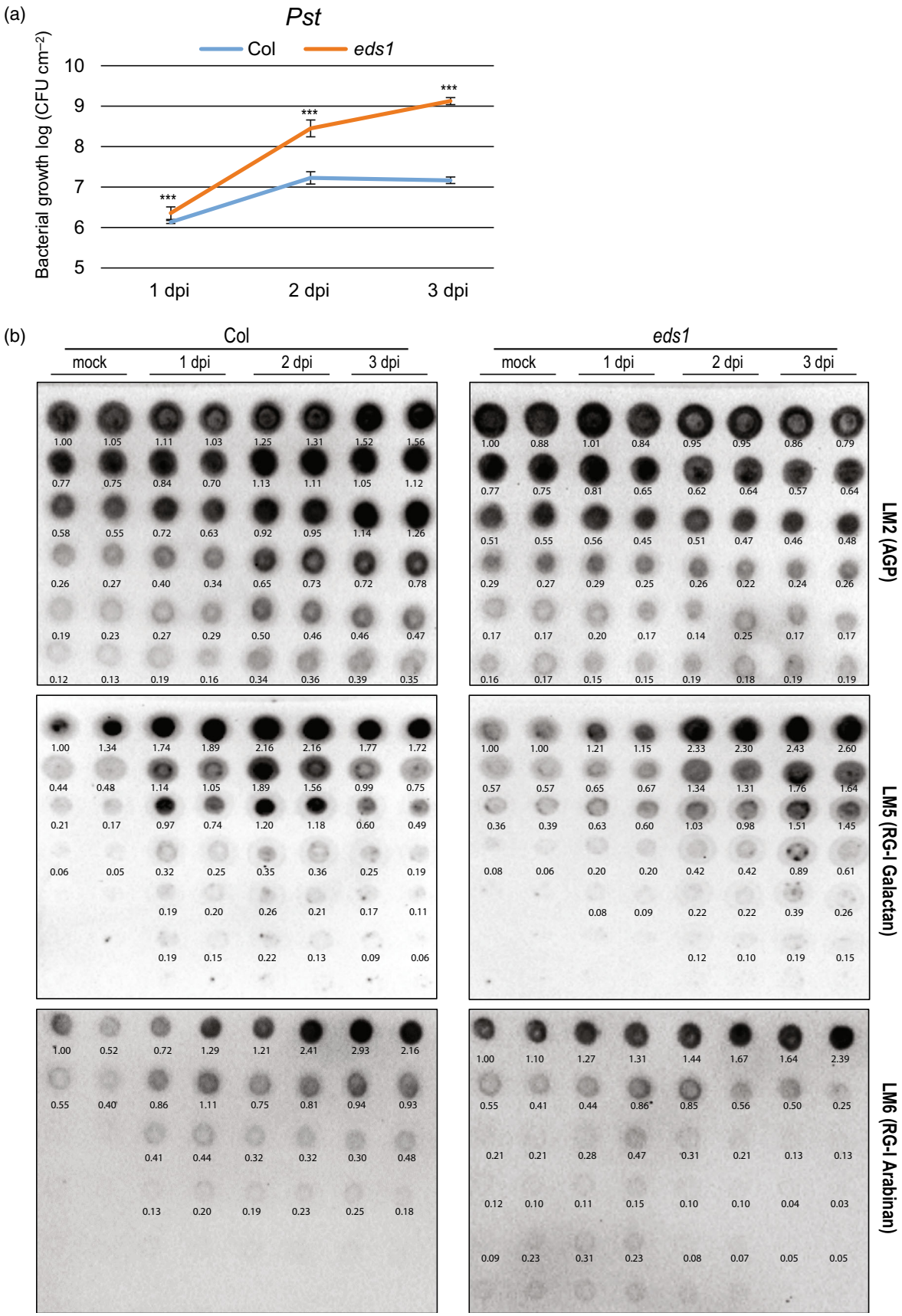

Figure 6. Spatio-temporal changes in CW correlate with dynamics of bacterial proliferation.
(a) Four-week-old Arabidopsis plants were infiltrated with *Pst* and bacterial titers were determined at 3 dpi. Data represent the mean of three biological replicates ± SE. Differences between genotypes were determined using Student's *t*-test ($P < 0.05$).
(b) Four-week-old Arabidopsis leaves of the indicated genotypes were infiltrated with *Pst*. Infiltrated leaves were harvested at 1, 2, and 3 dpi. Mock-treated plants were harvested at 3 dpi. Dot-blot analyses on 2 μg of 1 M KOH AIR (after extracting pectin fraction) with LM2 (AGP), LM6 (alpha-1,5-arabinan), LM5 (beta-1,4-galactan). Values represent the relative quantification of each dot-blot sample normalized to undiluted mock samples (value set to 1) within each blot.

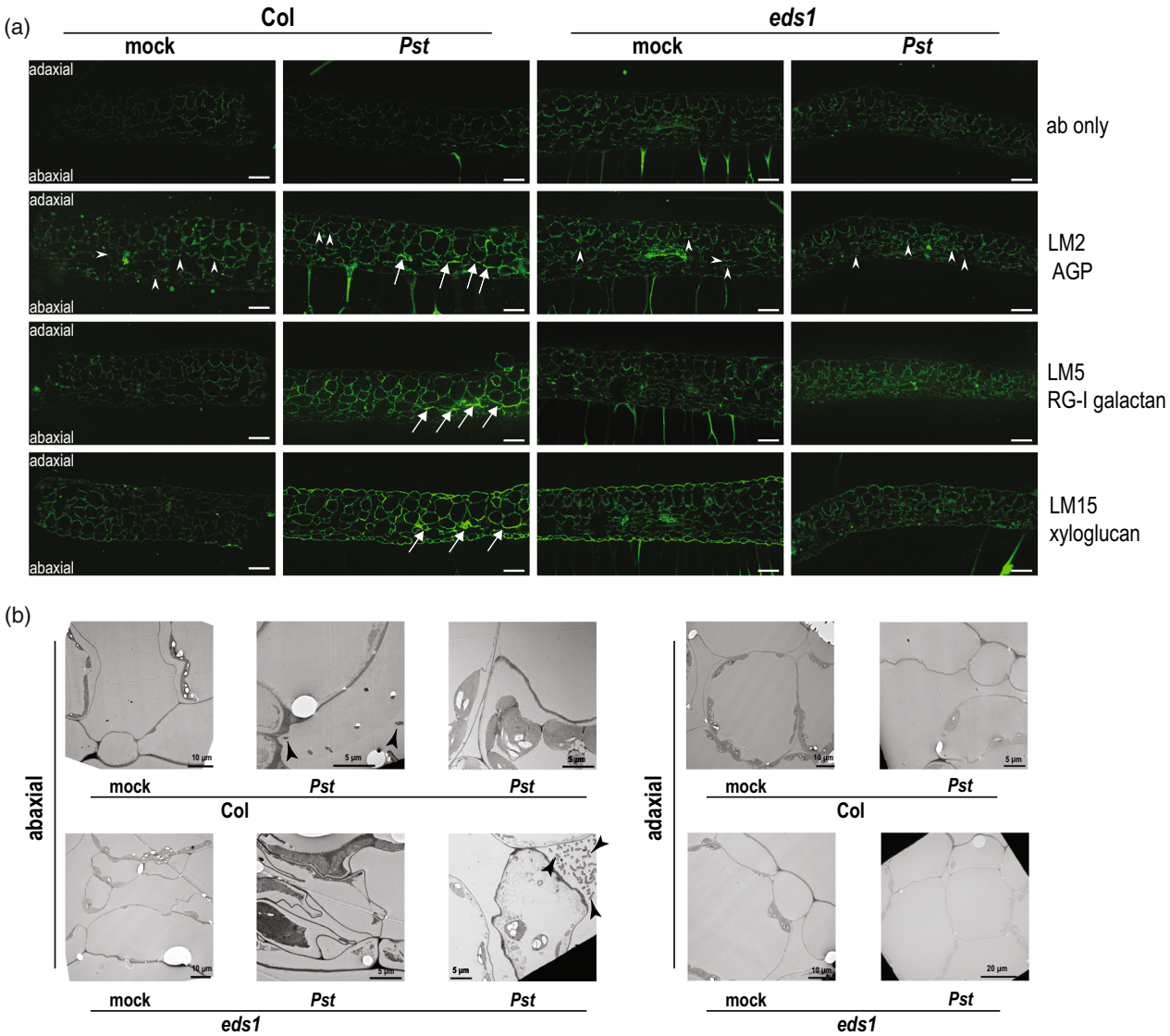

Figure 7. CW changes occur in the localized abaxial side of leaf.
(a) Four-week-old Arabidopsis plants of the indicated genotypes were infiltrated with either mock or *Pst*. Samples were harvested and fixed at 2 dpi. CW polymers were probed using antibodies against LM2 (AGP), LM5 (beta-1,4-galactan) and LM15 (xyloglucan). Stronger and localized signals were observed in the mesophyll cells of Col, but not *eds1*. Arrowheads indicate punctate labeling of LM2, and arrows indicate specific labeling in the sponge mesophyll cells in Col. Scale bar = 100 μm.
(b) TEM images of mock and *Pst*-infiltrated leaf tissue. Note the intact CW in Col and the shriveled CW in *eds1* on the abaxial side of the leaf only. Bacterial cells are indicated with arrowheads.

of Col, but not in *eds1* (Figure 7a). We did not observe such marked changes in the adaxial cells (Figure 7a). Consistent with CW labeling pattern upon *Pst* infection in the abaxial side of leaf, we found bacterial cells mostly in abaxial intercellular spaces (Figure 7b). As expected, we observed multiple bacterial colonies in *eds1*, but not in Col (Figure 7b). We also observed instances of shriveled CW organization in the abaxial side of *eds1* later in the

infection (3 dpi) but not in the adaxial side of the tissue (Figure 7b). These results point to CW modifications being limited to cells in contact with *Pst* rather than broadly in the tissue, supporting a local cell response, which is in agreement with our data for a lack of occurrence of systemic CW modifications (Figure 1b).

DISCUSSION

In addition to being a support structure, the CW is an interface between the protoplast and pathogens, which can modulate plant immunity (Underwood, 2012; Wolf et al., 2012). While CW modifications upon infection by penetrating fungal pathogens that have an arsenal of CW-degrading enzymes have been extensively studied (Dora et al., 2022; Kubicek et al., 2014), relatively little was known about CW modifications during the course of infection by bacteria, such as *Pst*, which reside in intercellular spaces. More specifically, it was not fully understood how, where, and to what extent the CW is modified during *Pst* infection and concomitant immune signaling. To address this significant gap in plant-pathogen interactions and contribute to the understanding of defense strategies actuated by the host, we systematically analyzed the changes in the CW NSC during a compatible interaction using the well-established *Pst-A. thaliana* system. Our study revealed that upon virulent infection the CW undergoes significant local modifications, which encompass an immune-independent accumulation of hexoses and an immune-dependent increase in pentoses, underscoring that the extensive and yet specific CW modifications are the combined result of both pathogen virulence and host immune responses. By analyzing CW modifications during disease progression, we also found significant changes in AGP deposition and attributed a critical requirement of APAP1 in immune responses. These results support that the CW undergoes specific local remodeling events and pinpoints specific polysaccharidic CW constituents as critical components in limiting pathogen growth.

To date, research on the role of the CW in plant immunity has been largely centered on identifying CW mutations that affect immune signaling or pathogen invasion (Malinovsky et al., 2014; Molina et al., 2021; Underwood, 2012; Wan et al., 2021). However, the underpinnings of, if and how, the plant immune response shapes the CW during the progression of the disease have not been defined yet. Significant lignin deposition has been verified in Col upon infection with *Pst* HrcC− and by avirulent *Pst* strains but not with *Pst* (Lee et al., 2019). Our work extends these findings by focusing on the analysis of the CW NSC. Particularly, we observed significant NSC changes in *Pst*-infected leaves of Col but not *eds1*, a mutant that lacks a central plant immunity component necessary to thwart pathogens (Lapin et al., 2020). The changes in NSC are unlikely attributable to increased bacterial cells because the most distinct NSC changes were observed in Col, which has reduced bacterial growth compared to *eds1*. In addition, a similar NSC alteration was also observed in *Pst* DC3000 Δcor-, which grew less on both Col and *eds1* compared to *Pst* (Figure S1). These results underscore that immune activation induces extensive CW changes that are not limited to lignin abundance (Lee et al., 2019) but also impact the NSC. Furthermore, we found that plants infected with *Pst* HrcC−, which is deficient in the type III secretion system (Yuan & He, 1996), did not manifest changes in CW NSC. Therefore, the observed CW changes are due to one or more effectors secreted by *Pst* and concomitant basal immune signaling activated to limit *Pst*. Our data are in line with the notion that *Pst* elicits effectors to subvert host immunity. An example is the *Pst* effector AvrPto, which suppresses callose deposition as part of a strategy to inhibit CW-based defense and enable the growth of *Pst* HrcC−. Future experiments quantifying NSC using different *Pst* effector mutants will be informative to understand how one or more of these effectors can affect CW-based defense. CW modifications by lignification (Lee et al., 2019) or alteration of the NSC (this work) might be tailored to specific pathogens and/or effectors. Although the identity of such effectors is yet unknown, by employing genetic tools, we were able to establish that the occurrence of CW NSC modifications is underpinned by different and specific requirements. For example, we showed that some of the NSC alterations, such as galactose and mannose, are due to pathogen-elicited coronatine, and we observed them only in infections with *Pst* but not with *Pst* DC3000 Δcor- (Figure 1d; Figure S1). Significantly, we established that, although SA plays a vital role in initiating SAR (Hartmann & Zeier, 2019), SA treatment alone did not result in extensive CW modifications, highlighting that extensive changes in CW due to *Pst* infection are likely the product of other signaling cues in addition to SA, including possible physical interactions between the CW and pathogens or CW damage by pathogens. This is in agreement with other studies showing that SA has a limited role in CW-based defense (Hauck et al., 2003; Molina et al., 2021).

Our analyses also identified two distinct modalities of CW NSC modifications due to pathogen virulence: (i) host immune-independent modifications, which lead to an increase in hexoses deposition, and (ii) host immune-dependent modifications, which lead to an increase in pentose levels, AGP deposition, and RG-I arabinan depletion. These results support that the observed NSC modifications that are consequent to pathogen infection are the combined result of immune-dependent and immune-independent responses by the host.

Pst infection hijacks organelles and intracellular signaling pathways to ensure bacterial proliferation and tissue propagation (Bhandari & Brandizzi, 2020; Dodds & Rathjen, 2010; Xin et al., 2018). We found that in the *eds1*

mutant, which allows higher *Pst* proliferation compared to Col, galactan levels were increased and correlated with increased expression of *GALS* transcripts. Conversely, *GALS* induction was attenuated early upon immune activation in Col. It has been shown that *Pseudomonas* strains favor sugars such as D-glucose and D-mannose for growth *in vitro* and *in vivo*, but nutrient limitation in the apoplast can drive bacteria to utilize unfavored sugars, such as D-galactose, as a carbon source (Rico & Preston, 2008). Early in infection, *Pst* perceives plant-derived factors as a signal to induce type III effectors, such as AvrPto (Anderson et al., 2014). Also, cultivation of *Pst* in minimal media supplemented with galactose has been shown to lead to the induction of AvrPto in *Pst* (Anderson et al., 2014). Therefore, the observed increase of the levels of hexose sugars in the CW NSC due to *Pst* infection is suggestive of pathogen-driven nutrient appropriation to favor bacterial growth and virulence, especially in a background such as *eds1*, which allows for high levels of bacterial infection. The clear increase of pentose levels in Col compared to the hypersusceptible mutants *sid2* and *eds1* underpins a role of immune signaling in pentose deposition. Compared to hexoses, pentoses are not preferred by bacteria, and the pentose metabolism in bacteria is energetically costly (Rico & Preston, 2008; Watanabe et al., 2019). Therefore, depositing more pentoses into the CW could represent a strategy of the host to make the CW less hospitable for *Pst* and thus potentially providing a hurdle to bacterial proliferation.

Among the increased pentoses, in this work, we found a remarkable increase in arabinose in the CW upon infection. Arabinose is commonly found in pectic polysaccharides, proteoglycan, and hemicelluloses such as arabinoxylan or xyloglucan. In addition, arabinose decorates AGPs, whose functions in the CW are not clearly understood yet (Showalter & Basu, 2016; Tan et al., 2013). Our results indicate preferential sequestration of the increased levels of arabinose into AGP deposition and not to RG-I arabinan. Because we observed a significant increase in AGP levels in *mur4*, which has almost undetectable RG-I arabinan and is more resistant to *Pst* (this work), degradation of RG-I arabinan does not appear necessary for AGP synthesis and plant immunity. AGPs are hypothesized to have roles in strengthening and monitoring CW and storing Ca^{2+} or transmitting Ca^{2+}-mediated signaling (Lamport & Várnai, 2013; Showalter & Basu, 2016). Thus, increased deposition of AGPs could either serve to attenuate immune signaling by quenching Ca^{2+} in the CW or act as sentinels to release Ca^{2+} upon perception of a pathogen attack. In addition, the verified immunity-driven deposition of AGPs in 4 M KOH fraction, where AGP is not usually found [(Pattathil et al., 2012) and this work], supports a structural role of AGPs in crosslinking different CW polymers, which may result in cordoning off pathogens. Indeed, we established that the loss of APAP1 leads to increased bacterial growth. It is plausible that, through a structural role in linking CW polysaccharides (Tan et al., 2013), APAP1 may restrict pathogen infection. This is in line with findings that AGP deposition is spatially regulated in response to different biotic interactions. For example, during infection by the gray mold *Botrytis cinerea*, a general increase of AGP levels and fraction-specific alteration of RG-I were observed in both wild type (resistant) and susceptible pectin methyl esterase mutants, indicative of pathogen-driven changes similar to our results (Lionetti et al., 2017). Therefore, AGP and RG-I modification could be a central target for CW modifications upon infection. Additionally, during infection by the another powdery mildew fungus *Golovinomyces orontii*, AGPs have been found excluded from a specialized PM structure, known as extrahaustorial membrane (EHM), which is formed during fungal invasion (Bozkurt & Kamoun, 2020; Micali et al., 2011). Nonetheless, AGPs were found to be part of the encasement surrounding the EHM (Micali et al., 2011), which suggests the role of AGPs in limiting pathogen penetration and highlights a specific spatial deposition of components in the CW. Thus, AGPs seemed to be recruited by both pathogens and plants to remodel CW. Notably, we found that AGP deposition occurs at later stages of *Pst* infection (i.e., days 2 and 3), which supports that AGP deposition is a late-stage immune event and likely a consequence of limiting pathogen growth.

CW fortification against invading fungal pathogens has been reported to occur at focal points of the infected tissue to limit pathogen spread (Chowdhury et al., 2016; Schmelzer, 2002). Our results support this notion as we found that *Pst* infection led to local CW changes in the infected leaves. Furthermore, we observed no CW changes in the systemic tissue, despite the activation of a systemic response. Therefore, systemic immunity actuated upon *Pst* infection is limited to intracellular signaling cascades that do not extend to changes in CW of systemic leaves despite the activation of systemic signaling.

In summary, our results support a novel model of spatiotemporal CW NSC modifications during *Pst* infection (Figure 8). The model envisions that the pathogen challenge induces remarkable changes in the NSC that are limited to focal regions in locally infected leaves (Figure 8a,b). Our results also support that the observed CW modifications are a function of pathogen-elicited effectors driving increased hexose deposition, including galactans (Figure 8c), an effect that is attenuated upon activation of immunity in Col but not in *eds1* (Figure 8d). In this model, activation of immunity leads to potentiation of defense pathways resulting in a depletion of RG-I arabinan but also in an increase in AGP deposition, including APAP1, which is necessary to mount a robust defense (Figure 8e). Further studies with different pathogens and effectors are likely to shed light on whether these are broadly conserved responses or evolved against specific pathogens.

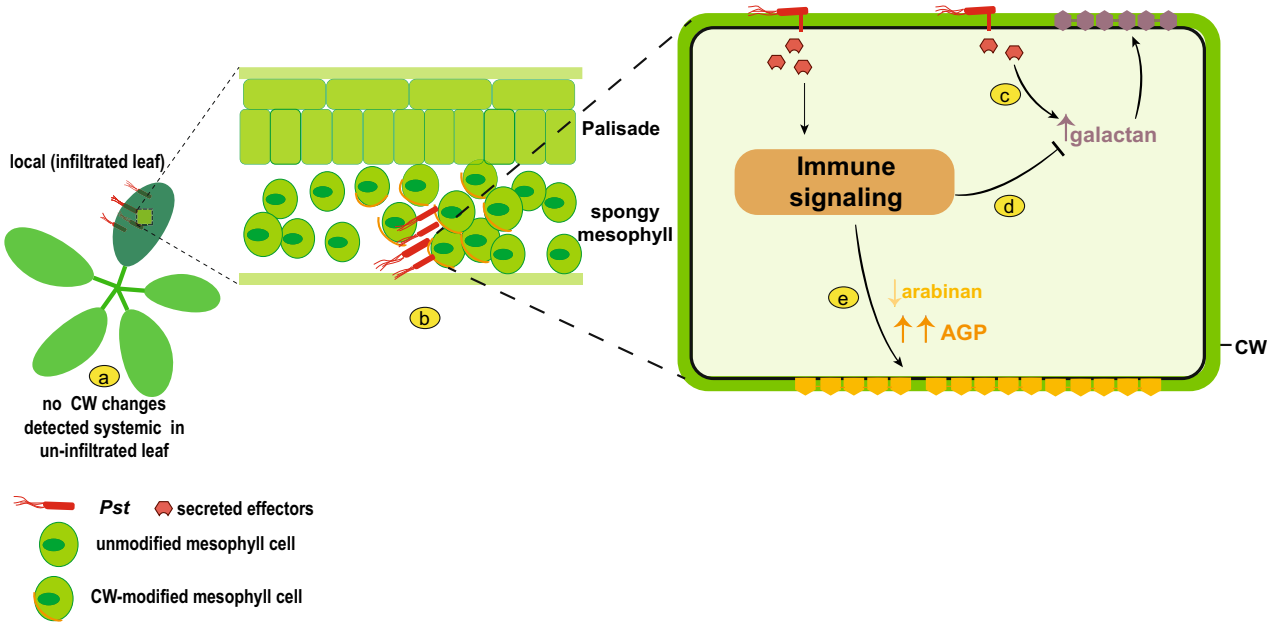

Figure 8. Model summarizing the CW NSC changes upon pathogen infection.
(a) *Pst*-driven CW changes are restricted to locally infiltrated leaves and not to systemic (uninfiltrated) leaves.
(b) CW modifications are limited to spongy mesophyll cells, likely because of direct contact with *Pst*.
(c) *Pst*-secreted effectors induce expression of galactan synthase genes leading to increased galactan deposition into the CW. Such increased galactan deposition is not observed in the type III secretion-deficient pathogen strain (*Pst* HrcC−).
(d) Activation of immune signaling in Col, but not in *eds1*, leads to attenuation of effector-driven galactan deposition.
(e) Activation of immune signaling cascades leads to increased deposition of arabinogalactan proteins (AGP) and depletion of RG-I arabinan. Image was generated using Biorender.

EXPERIMENTAL PROCEDURES

Plant materials, growth conditions, and pathogen strains

All mutants and lines were in Arabidopsis accession Col-0 background. The mutants *eds1-2*, *sid2-2*, *mur4-1*, *cslc4568 12*, and *apap1* were previously described (Bhandari et al., 2019; Kim et al., 2020; Tan et al., 2013; Wildermuth et al., 2002). *Pseudomonas syringae pv.* tomato (*Pst*) strain DC3000, *Pst hrcC*−, and *Pst* DC3000 Δcor- were used (Bhandari et al., 2019; Xin et al., 2018). Plants were grown on soil in controlled environment chambers under a 10 h light regime (120–150 μE m^{-2} sec^{-1}) at 22°C and 60% relative humidity.

Pathogen infection assays

For bacterial growth assays, *Pst* (OD600 = 0.0005) in 10 mM $MgCl_2$ was hand-infiltrated into leaves of four-week-old plants, and bacterial titers were measured, as described earlier (Bhandari et al., 2019). Each biological replicate is comprised of three leaf discs from different plants and data shown in each experiment is compiled from 3 to 4 biological replicates. Statistical analyses were performed using one-way ANOVA with post-hoc multiple testing correction using Tukey's HSD ($P < 0.05$).

qRT-PCR analyses

Total RNA was extracted using a Plant RNA extraction kit (Macherey-Nagel, Allentown, PA, USA). Five hundred nanograms of total RNA were used for cDNA synthesis (iScript) and qRT-PCR analyses were performed using SYBR green master mix. The housekeeping gene *GapDH* was used as a reference. Primer efficiencies were above 90% for all oligos, and data were analyzed by dCt to calculate relative expression. Primers used in this analysis are listed in Table S1.

Exogenous salicylic acid treatment

Arabidopsis seeds were surface-sterilized and plated on 0.5 MS with 1% sucrose. 10- to 12-day old seedlings were transferred to 0.5 MS with 1% sucrose plates supplemented with either 50 μM SA or DMSO. Samples were harvested at 3 dpi.

Cell wall analyses

Four-week-old Arabidopsis leaves from 25 plants were harvested after treatments, and immediately frozen in liquid N_2. Freeze-dried biomass was washed three times using each 70% ethanol and 1:1 chloroform/methanol, followed by washing with 100% acetone. Starch in the dried AIR was digested by α-amylase and pullanase. NSC was analyzed using three replicates from the pulled samples after producing alditol acetate derivatives of neutral sugars by TFA hydrolysis of de-starched AIR by GLBRC cell wall facility as described previously (Kim et al., 2015; York et al., 1986). Two independent experiments were performed.

The levels of uronic acids from mock or *Pst-treated* samples were estimated using the sulfamate/carbazole method using three biological replicates as described previously (Filisetti-Cozzi & Carpita, 1991).

Glycan array

Glycan array was performed as reported previously (Kim et al., 2020). Two replicates per each genotype are comprised of ~20

leaves from ~8 different plants. Glycan arrays were repeated at least twice. In this assay, sequentially extracted fractions from 2 mg of AIR were used. Chelating agent-soluble solids fraction (ChASS) was first isolated using a solution (50 mM Tris–HCl, 50 mM ammonium oxalate, and 50 mM trans-1,2-cyclohexanediaminetetraacetic acid (CDTA) at pH 7.2) with 2 mg of destarched AIR (10 mg ml^{-1}) (Francocci et al., 2013) prior to extraction of KOH fractions to avoid pectin de-methylesterification. KOH soluble fractions were extracted from the pellet (ChASS insoluble) using 1 and 4 M KOH with 20 mM $NaBH_4$ sequentially. Each KOH soluble fraction was neutralized with 50% acetic acid. To generate a dilution series, the ChASS fraction was diluted with ChASS solution with 0.25% (w/v) of oat β-glucan; the KOH fractions were diluted with 0.8 M KOH with 0.25% (w/v) of oat β-glucan. Primary antibodies (LM2, 1:500 dilution; LM5, 1:500 dilution; LM6, 1:500 dilution; LM10, 1:500 dilution; LM15, 1:500 dilution; JIM5, 1:500 dilution; JIM7, 1:500 dilution) in 1 × PBS with 0.5% non-fat dairy milk and secondary antibody (Rabbit anti-rat conjugated with HRP, 1:2000 dilution) in 1 × PBS with 0.5% non-fat dairy milk were used for the assay. For visualization, Supersignal West Femto maximum sensitivity substrate (www.thermofisher.com) was used for LM6 blotting, and Supersignal West pico maximum sensitivity substrate (www.thermofisher.com) was used for other antibodies. Dot blot signal intensity was quantified using Image Lab V6.1 software (Bio-Rad, Hercules, CA, USA). The software measured the signal intensity from each pixel inside equally sized areas for each dot. The background intensity was manually adjusted to obtain an accurate signal measurement. For all dilution series, the relative signal intensity of each dot was normalized to the mock control (top left dot, set to 1). For dilution series up to 0.05, the measurement data were presented below the respective dot in each image. Because of a low detectability of arabinan in the 4 M KOH, changes in arabinan were not quantified in the 4 M KOH fraction in Figures 3, 4, and Figure S5.

Immunofluorescence microscopy and transmission electron microscopy (TEM)

Four-week-old Arabidopsis leaves were fixed after treatment in 4% formaldehyde, 0.5% glutaraldehyde in 1 × PBS. Samples were dehydrated and embedded in LR white resin, then transverse sections (0.5 μm) were used for immunofluorescence, as previously described (Kim et al., 2015). As primary antibodies, LM2 (1:30), LM5 (1:30), and LM15 (1:30) were used. Goat anti-rat antibody conjugated with Alexa488 (1:100) was used as the secondary antibody.

For the TEM, ultra-thin sections (70 nm) were prepared from the samples used for immunofluorescence. The sections were post-stained with 2% uranyl acetate (w/v in water) for 5 min and 1% lead citrate for 2 min and visualized using JEOL 1400 Flash Electron Microscope.

Antibodies

The antibodies adopted in this work were procured from PlantProbes and Kerafast. A detailed information is available at https://plantcellwalls.leeds.ac.uk/wp-content/uploads/sites/103/2021/11/JPKab2021.pdf

ACKNOWLEDGEMENTS

We thank Drs. Debra Mohnen (University of Georgia) and Walter Gassmann (University of Missouri) for *apap1* and *eds1-2* mutant seeds, respectively. We thank Dr. Sheng Yang He (Duke University) for providing *Pseudomonas* strains. We thank the GLBRC cell wall facility for cell wall composition analysis. We thank colleagues in the Brandizzi lab for helpful discussions. This work was funded primarily by the DOE Great Lakes Bioenergy Research Center (DOE BER Office of Science DE-SC0018409) and the Michigan State University Research Foundation. We also acknowledge partial support from the Chemical Sciences, Geosciences and Biosciences Division, Office of Basic Energy Sciences, Office of Science, US Department of Energy (award number DE-FG02-91ER20021), National Science Foundation (MCB1727362) and AgBioResearch (MICL02598) to FB.

AUTHOR CONTRIBUTIONS

DDB, SJK, and FB designed the study; DDB, SJK, and RS performed experiments; DDB, SJK, and FB analyzed and interpreted the data and wrote the manuscript.

CONFLICT OF INTEREST

The authors have no conflict of interest.

SUPPORTING INFORMATION

Additional Supporting Information may be found in the online version of this article.

Figure S1. *Pst* infection leads to CW changes in local but not systemic tissue.

Figure S2. Level of xyloglucan and heteroxylan were not significantly altered upon *Pst* infection.

Figure S3. Differential sequestration of arabinose upon *Pst* infection.

Figure S4. Spatiotemporal changes in CW composition correlate with dynamics of bacterial proliferation.

Figure S5. Spatiotemporal changes in the 4 M CW fraction correlate with dynamics of bacterial proliferati1on.

Figure S6. *Pst* causes demethylation of pectin.

Figure S7. Transcript levels of genes involved in AGP and RG-I are changed upon *Pst* infection.

Figure S8. CW changes occur in the localized abaxial side of an infected leaf.

Table S1. Primers.

REFERENCES

Aarts, N., Metz, M., Holub, E., Staskawicz, B.J., Daniels, M.J. & Parker, J.E. (1998) Different requirements for EDS1 and NDR1 by disease resistance genes define at least two R gene-mediated signaling pathways in Arabidopsis. *Proceedings of the National Academy of Sciences of the United States of America*, **95**, 10306–10311.

Anderson, J.C., Wan, Y., Kim, Y.M., Pasa-Tolic, L., Metz, T.O. & Peck, S.C. (2014) Decreased abundance of type III secretion systeminducing signals in Arabidopsis mkp1 enhances resistance against *Pseudomonas syringae*. *Proceedings of the National Academy of Sciences of the United States of America*, **111**, 6846–6851.

Bethke, G., Thao, A., Xiong, G., Li, B., Soltis, N.E., Hatsugai, N. *et al.* (2015) Pectin biosynthesis is critical for cell wall integrity and immunity in Arabidopsis thaliana. *Plant Cell*, **28**, 537–556.

Bhandari, D.D. & Brandizzi, F. (2020) Plant endomembranes and cytoskeleton: moving targets in immunity. *Current Opinion in Plant Biology*, **58**, 8–16. Available from: https://doi.org/10.1016/j.pbi.2020.09.003

Bhandari, D.D., Lapin, D., Kracher, B., von Born, P., Bautor, J., Niefind, K. *et al.* (2019) An EDS1 heterodimer signalling surface enforces timely reprogramming of immunity genes in Arabidopsis. *Nature Communications*, **10**, 772.

Borassi, C., Sede, A.R., Mecchia, M.A., Salgado Salter, J.D., Marzol, E., Muschietti, J.P. *et al.* (2016) An update on cell surface proteins containing extensin-motifs. *Journal of Experimental Botany*, **67**, 477–487.

Bozkurt, T.O. & **Kamoun, S.** (2020) The plant-pathogen haustorial interface at a glance. *Journal of Cell Science*, **133**, jcs237958.

Burget, E.G., **Verma, R.**, **Mølhøj, M.** & **Reiter, W.D.** (2003) The biosynthesis of L-arabinose in plants: molecular cloning and characterization of a golgi-localized UDP-D-xylose 4-epimerase encoded by the MUR4 gene of arabidopsis. *Plant Cell*, **15**, 523–531.

Cannon, M.C., **Terneus, K.**, **Hall, Q.**, **Tan, L.**, **Wang, Y.**, **Wegenhart, B.L.** ***et al.*** (2008) Self-assembly of the plant cell wall requires an extensin scaffold. *Proceedings of the National Academy of Sciences of the United States of America*, **105**, 2226–2231.

Chowdhury, J., **Schober, M.S.**, **Shirley, N.J.**, **Singh, R.R.**, **Jacobs, A.K.**, **Douchkov, D.** ***et al.*** (2016) Down-regulation of the *glucan synthase-like 6* gene (HvGsl6) in barley leads to decreased callose accumulation and increased cell wall penetration by *Blumeria graminis* f. sp. hordei. *The New Phytologist*, **212**, 434–443.

Couto, D. & **Zipfel, C.** (2016) Regulation of pattern recognition receptor signalling in plants. *Nature Reviews. Immunology*, **16**, 537–552.

Cui, H., **Qiu, J.**, **Zhou, Y.**, **Bhandari, D.D.**, **Zhao, C.**, **Bautor, J.** ***et al.*** (2018) Antagonism of transcription factor MYC2 by EDS1/PAD4 complexes bolsters salicylic acid defense in arabidopsis effector-triggered immunity. *Molecular Plant*, **11**, 1053–1066.

Cui, H., **Tsuda, K.** & **Parker, J.E.** (2015) Effector-triggered immunity: from pathogen perception to robust defense. *Annual Review of Plant Biology*, **66**, 487–511.

De Lorenzo, G., **Ferrari, S.**, **Giovannoni, M.**, **Mattei, B.** & **Cervone, F.** (2019) Cell wall traits that influence plant development, immunity, and bioconversion. *The Plant Journal*, **97**, 134–147.

Dewdney, J., **Lynne Reuber, T.**, **Wildermuth, M.C.**, **Devoto, A.**, **Cui, J.**, **Stutius, L.M.** ***et al.*** (2000) Three unique mutants of Arabidopsis identify eds loci required for limiting growth of a biotrophic fungal pathogen. *The Plant Journal*, **24**, 205–218.

Ding, P. & **Ding, Y.** (2020) Stories of salicylic acid: a plant defense hormone. *Trends in Plant Science*, **25**, 549–565. Available from: https://doi.org/10.1016/j.tplants.2020.01.004

Dodds, P.N. & **Rathjen, J.P.** (2010) Plant immunity: towards an integrated view of plant–pathogen interactions. *Nature Reviews. Genetics*, **11**, 539–548.

Dora, S., **Terrett, O.M.** & **Sánchez-Rodríguez, C.** (2022) Plant–microbe interactions in the apoplast: communication at the plant cell wall. *Plant Cell*, **34**, 1532–1550.

Engelsdorf, T., **Will, C.**, **Hofmann, J.**, **Schmitt, C.**, **Merritt, B.B.**, **Rieger, L.** ***et al.*** (2017) Cell wall composition and penetration resistance against the fungal pathogen Colletotrichum higginsianum are affected by impaired starch turnover in Arabidopsis mutants. *Journal of Experimental Botany*, **68**, 701–713.

Filisetti-Cozzi, T.M.C.C. & **Carpita, N.C.** (1991) Measurement of uronic acids without interference from neutral sugars. *Analytical Biochemistry*, **197**, 157–162.

Francocci, F., **Bastianelli, E.**, **Lionetti, V.**, **Ferrari, S.**, **De Lorenzo, G.**, **Bellincampi, D.** ***et al.*** (2013) Analysis of pectin mutants and natural accessions of Arabidopsis highlights the impact of de-methyl-esterified homogalacturonan on tissue saccharification. *Biotechnology for Biofuels*, **6**, 4–11.

Gaspar, Y.M., **Nam, J.**, **Schultz, C.J.**, **Lee, L.Y.**, **Gilson, P.R.**, **Gelvin, S.B.** ***et al.*** (2004) Characterization of the arabidopsis lysine-rich arabinogalactan-protein AtAGP17 mutant (rat1) that results in a decreased efficiency of agrobacterium transformation. *Plant Physiology*, **135**, 2162–2171.

Gille, S. & **Pauly, M.** (2012) O-acetylation of plant cell wall polysaccharides. *Frontiers in Plant Science*, **3**, 1–7.

Hartmann, M. & **Zeier, J.** (2019) N-hydroxypipecolic acid and salicylic acid: a metabolic duo for systemic acquired resistance. *Current Opinion in Plant Biology*, **50**, 44–57.

Hartmann, M., **Zeier, T.**, **Bernsdorff, F.**, **Reichel-Deland, V.**, **Kim, D.**, **Hohmann, M.** ***et al.*** (2018) Plant systemic immunity Flavin monooxygenase-generated N-Hydroxypipecolic acid is a critical element of plant systemic immunity. *Cell*, **173**, 456–469.

Hauck, P., **Thilmony, R.** & **He, S.Y.** (2003) A *Pseudomonas syringae* type III effector suppresses cell wall-based extracellular defense in susceptible Arabidopsis plants. *Proceedings of the National Academy of Sciences of the United States of America*, **100**, 8577–8582.

Hernández-Blanco, C., **Feng, D.X.**, **Hu, J.**, **Sánchez-Vallet, A.**, **Deslandes, L.**, **Llorente, F.** ***et al.*** (2007) Impairment of cellulose synthases required for Arabidopsis secondary cell wall formation enhances disease resistance. *Plant Cell*, **19**, 890–903.

Jones, J.D.G. & **Dangl, J.L.** (2006) The plant immune system. *Nature*, **444**, 323–329.

Jones, L., **Seymour, G.B.** & **Knox, J.P.** (1997) Localization of pectic galactan in tomato cell walls using a monoclonal antibody specific to (1→4)-β-D-galactan. *Plant Physiology*, **113**, 1405–1412.

Kaur, D., **Held, M.A.**, **Smith, M.R.** & **Showalter, A.M.** (2021) Functional characterization of hydroxyproline-O-galactosyltransferases for Arabidopsis arabinogalactan-protein synthesis. *BMC Plant Biology*, **21**, 1–24. Available from: https://doi.org/10.1186/s12870-021-03362-2

Kim, S.J., **Chandrasekar, B.**, **Rea, A.C.**, **Danhof, L.**, **Zemelis-Durfee, S.**, **Thrower, N.** ***et al.*** (2020) The synthesis of xyloglucan, an abundant plant cell wall polysaccharide, requires CSLC function. *Proceedings of the National Academy of Sciences of the United States of America*, **117**, 20316–20324.

Kim, S.J., **Held, M.A.**, **Zemelis, S.**, **Wilkerson, C.** & **Brandizzi, F.** (2015) CGR2 and CGR3 have critical overlapping roles in pectin methylesterification and plant growth in Arabidopsis thaliana. *The Plant Journal*, **82**, 208–220.

Kubicek, C.P., **Starr, T.L.** & **Glass, N.L.** (2014) Plant cell wall-degrading enzymes and their secretion in plant-pathogenic fungi. *Annual Review of Phytopathology*, **52**, 427–451.

Lamport, D.T.A. & **Várnai, P.** (2013) Periplasmic arabinogalactan glycoproteins act as a calcium capacitor that regulates plant growth and development. *The New Phytologist*, **197**, 58–64.

Lapin, D., **Bhandari, D.D.** & **Parker, J.E.** (2020) Origins and immunity networking functions of EDS1 family proteins. *Annual Review of Phytopathology*, **58**, 253–276.

Lee, M., **Jeon, H.S.**, **Kim, S.H.** ***et al.*** (2019) Lignin-based barrier restricts pathogens to the infection site and confers resistance in plants. *The EMBO Journal*, **38**, 1–17.

Lionetti, V., **Cervone, F.** & **Bellincampi, D.** (2012) Methyl esterification of pectin plays a role during plant-pathogen interactions and affects plant resistance to diseases. *Journal of Plant Physiology*, **169**, 1623–1630. Available from: https://doi.org/10.1016/j.jplph.2012.05.006

Lionetti, V., **Fabri, E.**, **De Caroli, M.**, **Hansen, A.R.**, **Willats, W.G.T.**, **Piro, G.** ***et al.*** (2017) Three pectin methylesterase inhibitors protect cell wall integrity for arabidopsis immunity to botrytis. *Plant Physiology*, **173**, 1844–1863.

Malinovsky, F.G., **Fangel, J.U.** & **Willats, W.G.T.** (2014) The role of the cell wall in plant immunity. *Frontiers in Plant Science*, **5**, 1–12.

Manohar, M., **Tian, M.**, **Moreau, M.**, **Park, S.W.**, **Choi, H.W.**, **Fei, Z.** ***et al.*** (2015) Identification of multiple salicylic acid-binding proteins using two high throughput screens. *Frontiers in Plant Science*, **5**, 1–14.

Marcus, S.E., **Verhertbruggen, Y.**, **Hervé, C.**, **Ordaz-Ortiz, J.J.**, **Farkas, V.**, **Pedersen, H.L.** ***et al.*** (2008) Pectic homogalacturonan masks abundant sets of xyloglucan epitopes in plant cell walls. *BMC Plant Biology*, **8**, 1–12.

Mareri, L., **Romi, M.** & **Cai, G.** (2019) Arabinogalactan proteins: actors or spectators during abiotic and biotic stress in plants? *Plant Biosystems*, **153**, 173–185. Available from: https://doi.org/10.1080/11263504.2018.1473525

McCartney, L., **Marcus, S.E.** & **Knox, J.P.** (2005) Monoclonal antibodies to plant cell wall xylans and arabinoxylans. *The Journal of Histochemistry and Cytochemistry*, **53**, 543–546.

Micali, C.O., **Neumann, U.**, **Grunewald, D.**, **Panstruga, R.** & **O'Connell, R.** (2011) Biogenesis of a specialized plant-fungal interface during host cell internalization of *Golovinomyces orontii* haustoria. *Cellular Microbiology*, **13**, 210–226.

Molina, A., **Miedes, E.**, **Bacete, L.**, **Rodríguez, T.**, **Mélida, H.**, **Denancé, N.** ***et al.*** (2021) Arabidopsis cell wall composition determines disease resistance specificity and fitness. *Proceedings of the National Academy of Sciences of the United States of America*, **118**, 1–12.

Pattathil, S., **Avci, U.**, **Miller, J.S.** & **Hahn, M.G.** (2012) Immunological approaches to plant cell wall and biomass characterization: glycome profiling. *Methods in Molecular Biology*, **908**, 61–72.

Pogorelko, G., **Lionetti, V.**, **Fursova, O.**, **Sundaram, R.M.**, **Qi, M.**, **Whitham, S.A.** ***et al.*** (2013) Arabidopsis and *Brachypodium distachyon* transgenic plants expressing *Aspergillus nidulans* acetylesterases have decreased degree of polysaccharide acetylation and increased resistance to pathogens. *Plant Physiology*, **162**, 9–23.

Pontiggia, D., **Benedetti, M.**, **Costantini, S.**, **De Lorenzo, G.** & **Cervone, F.** (2020) Dampening the DAMPs: how plants maintain the homeostasis of cell wall molecular patterns and avoid hyper-immunity. *Frontiers in Plant Science*, **11**, 613259.

Rico, A. & **Preston, G.M.** (2008) *Pseudomonas syringae* pv. Tomato DC3000 uses constitutive and apoplast-induced nutrient assimilation pathways to catabolize nutrients that are abundant in the tomato apoplast. *Molecular Plant-Microbe Interactions*, **21**, 269–282.

Scheller, H.V. & **Ulvskov, P.** (2010) Hemicelluloses. *Annual Review of Plant Biology*, **61**, 263–289.

Schmelzer, E. (2002) Cell polarization, a crucial process in fungal defence. *Trends in Plant Science*, **7**, 411–415.

Sels, J., **Mathys, J.**, **De Coninck, B.M.A.**, **Cammue, B.P.A.** & **De Bolle, M.F.C.** (2008) Plant pathogenesis-related (PR) proteins: a focus on PR peptides. *Plant Physiology and Biochemistry*, **46**, 941–950.

Sherson, S., **Gy, I.**, **Medd, J.**, **Schmidt, R.**, **Dean, C.**, **Kreis, M.** ***et al.*** (1999) The arabinose kinase, ARA1, gene of Arabidopsis is a novel member of the galactose kinase gene family. *Plant Molecular Biology*, **39**, 1003–1012.

Showalter, A.M. & **Basu, D.** (2016) Extensin and arabinogalactan-protein biosynthesis: glycosyltransferases, research challenges, and biosensors. *Frontiers in Plant Science*, **7**, 814.

Smallwood, M., **Yates, E.A.**, **Willats, W.G.T.**, **Martin, H.** & **Knox, J.P.** (1996) Immunochemical comparison of membrane-associated and secreted arabinogalactan-proteins in rice and carrot. *Planta*, **198**, 452–459.

Swaminathan, S., **Lionetti, V.** & **Zabotina, O.A.** (2022) Plant cell wall integrity perturbations and priming for defense. *Plants*, **11**, 1–26.

Tan, L., **Eberhard, S.**, **Pattathil, S.**, **Warder, C.**, **Glushka, J.**, **Yuan, C.** ***et al.*** (2013) An Arabidopsis cell wall proteoglycan consists of pectin and arabinoxylan covalently linked to an arabinogalactan protein. *Plant Cell*, **25**, 270–287.

Thordal-Christensen, H. (2020) A holistic view on plant effector-triggered immunity presented as an iceberg model. *Cellular and Molecular Life Sciences*, **77**, 3963–3976. Available from: https://doi.org/10.1007/s00018-020-03515-w

Tsuda, K., **Sato, M.**, **Stoddard, T.**, **Glazebrook, J.** & **Katagiri, F.** (2009) Network properties of robust immunity in plants. *PLoS Genetics*, **5**, e1000772.

Underwood, W. (2012) The plant cell wall: a dynamic barrier against pathogen invasion. *Frontiers in Plant Science*, **3**, 1–6.

van der Burgh, A.M. & **Joosten, M.H.A.J.** (2019) Plant immunity: thinking outside and inside the box. *Trends in Plant Science*, **24**, 587–601. Available from: https://doi.org/10.1016/j.tplants.2019.04.009

Vlad, F., **Spano, T.**, **Vlad, D.**, **Bou Daher, F.**, **Ouelhadj, A.** & **Kalaitzis, P.** (2007) Arabidopsis prolyl 4-hydroxylases are differentially expressed in response to hypoxia, anoxia and mechanical wounding. *Physiologia Plantarum*, **130**, 471–483.

Vogel, J.P., **Raab, T.K.**, **Somerville, C.R.** & **Somerville, S.C.** (2004) Mutations in PMR5 result in powdery mildew resistance and altered cell wall composition. *The Plant Journal*, **40**, 968–978.

Wan, J., **He, M.**, **Hou, Q.**, **Zou, L.**, **Yang, Y.**, **Wei, Y.** ***et al.*** (2021) Cell wall associated immunity in plants. *Stress Biology*, **1**, 1–15.

Watanabe, S., **Fukumori, F.**, **Nishiwaki, H.**, **Sakurai, Y.**, **Tajima, K.** & **Watanabe, Y.** (2019) Novel non-phosphorylative pathway of pentose metabolism from bacteria. *Scientific Reports*, **9**, 1–12.

Wildermuth, M.C., **Dewdney, J.**, **Wu, G.** & **Ausubel, F.M.** (2002) Erratum: isochorismate synthase is required to synthesize salicylic acid for plant defence (nature (2001) 414 (562–565)). *Nature*, **417**, 571.

Willats, W.G.T., **Marcus, S.E.** & **Knox, J.P.** (1998) Generation of a monoclonal antibody specific to (1->5) -alpha- arabinan. *Carbohydrate Research*, **308**, 149–152.

Winter, D., **Vinegar, B.**, **Nahal, H.**, **Ammar, R.**, **Wilson, G.V.** & **Provart, N.J.** (2007) An "electronic fluorescent pictograph" browser for exploring and analyzing large-scale biological data sets. *PLoS One*, **2**, 1–12.

Wolf, S. (2022) Cell Wall signaling in plant development and defense. *Annual Review of Plant Biology*, **73**, 1–31.

Wolf, S., **Hématy, K.** & **Höfte, H.** (2012) Growth control and cell wall signaling in plants. *Annual Review of Plant Biology*, **63**, 381–407.

Wu, Y., **Zhang, D.**, **Chu, J.Y.**, **Boyle, P.**, **Wang, Y.**, **Brindle, I.D.** ***et al.*** (2012) The Arabidopsis NPR1 protein is a receptor for the plant defense hormone salicylic acid. *Cell Reports*, **1**, 639–647.

Xin, X.F., **Kvitko, B.** & **He, S.Y.** (2018) *Pseudomonas syringae*: what it takes to be a pathogen. *Nature Reviews. Microbiology*, **16**, 316–328. Available from: https://doi.org/10.1038/nrmicro.2018.17

Yang, J. & **Showalter, A.M.** (2007) Expression and localization of AtAGP18, a lysine-rich arabinogalactan- protein in Arabidopsis. *Planta*, **226**, 169–179.

Yates, E.A., **Valdor, J.F.**, **Haslam, S.M.**, **Morris, H.R.**, **Dell, A.**, **Mackie, W.** ***et al.*** (1996) Characterization of carbohydrate structural features recognized by anti-arabinogalactan-protein monoclonal antibodies. *Glycobiology*, **6**, 131–139.

York, W.S., **Darvill, A.G.**, **McNeil, M.**, **Stevenson, T.T.** & **Albersheim, P.** (1986) Isolation and characterization of plant cell walls and cell wall components. *Methods in Enzymology*, **118**, 3–40.

Yuan, J. & **He, S.Y.** (1996) The *Pseudomonas syringae* Hrp regulation and secretion system controls the production and secretion of multiple extracellular proteins. *Journal of Bacteriology*, **178**, 6399–6402.

Zhang, Y. & **Li, X.** (2019) Salicylic acid: biosynthesis, perception, and contributions to plant immunity. *Current Opinion in Plant Biology*, **50**, 29–36.

Zhang, Y., **Yang, J.** & **Showalter, A.M.** (2011) AtAGP18 is localized at the plasma membrane and functions in plant growth and development. *Planta*, **233**, 675–683.

Zhou, F., **Emonet, A.**, **Dénervaud Tendon, V.**, **Marhavy, P.**, **Wu, D.**, **Lahaye, T.** ***et al.*** (2020) Co-incidence of damage and microbial patterns controls localized immune responses in roots. *Cell*, **180**, 440–453.e18.